Original article

Institution of MECHANICAL ENGINEERS
Journal of PROCESS MECHANICAL ENGINEERING

Proc IMechE Part E:
J Process Mechanical Engineering
1–15
© IMechE 2023
Article reuse guidelines:
sagepub.com/journals-permissions
DOI: 10.1177/09544089231154350
journals.sagepub.com/home/pie
SAGE

An experimental study on the determination of a hermetic reciprocating compressor's discharge and suction losses

Aykut Bacak[1,2], Ali Pınarbaşı[1] and Ahmet Selim Dalkılıç[1]

The most popular approach to determine compressor losses is to generate compressor pressure-volume indication diagrams. The pressure-volume indication diagram of a novel hermetic reciprocating compressor for household refrigerators operating with R600a was experimentally obtained under American Society of Heating, Refrigerating and Air-Conditioning Engineers (54.4°C/−23.3°C) and additional specific working conditions of (40°C/−25°C), (25°C/−20°C) and (35°C/−15°C). Apart from most studies, experiments have been performed using a calorimeter. The alteration of suction and discharge pressures with crank angle of the investigated compressor was presented as both graphical and numerical information during condensation and evaporation, separately. As a result of the analyses, total compressor losses increased with decreasing the condensation pressure. These losses were 10%, 8.7%, 5.7% and 4.6% of the total work and they were observed at the same speed of 1300 rotation per minute (rpm) as the lowest one under all operating conditions. Besides, the suction line losses having the largest losses in the compressor were calculated as 50.1%, 50.9%, 64.9% and 67.9% of the total one, and it has been determined that they increased with increasing the condensation pressure. Due to the more complex design of the equipment in the suction line, the losses in this region were found to be higher than those in the discharge line, as expected.

Keywords
Hermetic reciprocating compressor, pV indicator diagram, discharge losses, suction losses

Date received: 26 November 2022; accepted: 15 January 2023

Introduction

As life quality and consumption have been increasing, appliances such as refrigerators, air conditioners and other household equipment have been commonly used and considered as a fundamental need. These appliances already account for 50% of overall household electricity use. Refrigerators, air conditioners and other equipment for refrigeration and heating demand higher performance standards in some situations that promote energy savings and emission reduction. Due to refrigerator regulations and intensifying competition, household appliance compressors are supposed to be inexpensive, highly efficient, low in vibration and compact. The compressor is the most electricity-using component in domestic refrigerators; its energy efficiency is affected by thermodynamic, mechanical and electrical losses. Therefore, it is vital to eliminate these losses to maximize efficiency. Compressors for hermetic refrigeration are essential components of home appliances. The research and development of hermetic refrigeration compressors have taken the attention of scholars recently. Many studies on the simulations and experiments of the constant and variable speed compressors' efficiency have been undertaken, as mentioned below.

To facilitate sensor placement, the refrigerator's compressor was modified by Zhang et al.[1] They evaluated the compressor's performance in a single operating condition as well as in laboratory conditions. Three pressure sensors were fitted to monitor the pressure-volume (pV) diagram and pressure pulsation, and a strain gauge was utilized to measure the movement of the suction valve by considering the oil stiction effect. The results of the experiment revealed the relationship between pressure difference and valve movement. Under experimental conditions, it was established that the suction procedure led to a power loss of up to 14.5%. In addition, they noted that there was a delay in the opening of the suction reed valve due to losses in the suction muffler.

Real and Pereira[2] measured the synchronized pV diagram of a reciprocating refrigeration compressor and

[1]Department of Mechanical Engineering, Faculty of Mechanical Engineering, Yildiz Technical University, Istanbul, Turkey
[2]Department of Thermodynamics and System Based Modelling, Research and Development Center, Arçelik A.Ş., Istanbul, Turkey

Corresponding author:
Aykut Bacak, Department of Mechanical Engineering, Faculty of Mechanical Engineering, Yildiz Technical University, 34349 Istanbul, Turkey.
Email: aykut.bacak@arcelik.com

its valve operation. They produced a pV diagram of a reciprocating refrigerating compressor that was synced with its valve operation, and backflow effects were verified. They stated that it can be gained a better knowledge of the valves' losses and confirmed the gas backflow in its entirety by measuring the pV and the valve's operation. They produced a pV diagram of a reciprocating refrigerating compressor that was synced with its valve operation, and backflow effects were verified.

Jin et al.[3] proposed a detrending extracting zooming (DEZ) method to measure the rotational speed of a hermetic reciprocating compressor for a single case under laboratory conditions. The fluid-structure interaction (FSI) model was established, and the mechanism of pressure pulsation creation was examined. Based on numerical simulations at various operating speeds, the influence laws of pressure pulsation were determined. The trend component and harmonic components of pressure pulsation have been discovered to influence the estimate of rotational frequency. The DEZ reduced the trend component of pressure pulsation before extracting the feature component and enhancing the spectral resolution without sacrificing real-time performance.

Egger et al.[4] developed a cost-effective solution for a suction reed valve with mechanical assistance for an industrial compressor. They analyzed valve movements experimentally under calorimetric operating settings and constructed a mathematical model to study the influence of a situation at different operating speeds in the study. The concept consisted of a typical reed valve and a simple valve support mechanism. Several design variants were optimized based on a multi-response optimization strategy following an initial proof of concept. The study discovered that the valve leaf of varied design parameters opens early or late, with the best benefit realized for a compressor speed of up to 5000 rpm.

Silva and Dutra[5] employed a simulation model based on a non-steady lumped version of the mass and energy conservation equations to forecast the piston trajectory that results in the maximum thermodynamic efficiency for a reciprocating compressor while ignoring the restrictions of the driving mechanism under a single operating condition. The optimal piston trajectory (OPT) was composed of four constant-speed phases of the piston and results in shorter expansion, suction and discharge periods than a conventional crank-rod compressor, but a longer compression time. The OPT enhanced its thermodynamic efficiency from 88.3% to 92.1% and its volumetric efficiency from 70.9% to 72.0%, mostly as a result of decreased heat transfer and leakage losses.

Posch et al.[6] characterized compressor losses in terms of entropy production and exergy loss for a household reciprocating compressor under a single operating condition. According to their location, the findings were segmented into losses. The application of the methodology to a compressor with a cooled valve plate revealed that the cooling capacity of the compressor at American Society of Heating, Refrigerating and Air-Conditioning Engineers (ASHRAE) test conditions could be increased by 2.63%, but the compressor's coefficient of performance (COP) was only increased by 1.57% due to the increase in viscosity-related mechanical losses.

To realize the independent motion of each valve plate in a three-dimensional (3D) computational fluid dynamics (CFD) model of a double-acting industrial reciprocating compressor, Zhao et al.[7] proposed a mesh mapping approach. Consequently, both the transient flow within the compressor and the interaction between valve motion and pressure pulsation might be managed simultaneously under a single operating condition. In addition, the re-normalization group (RNG) k-model and the detached eddy simulation (DES) model were used to evaluate their influence on pressure pulsation. The RNG k-ϵ model successfully predicted pressure pulsation below 500 Hz, as revealed by an FFT study. At 420 rpm, the DES model was capable of resolving substantially higher frequencies than 1500 Hz within a 10% error margin.

Collings and Lenz[8] studied whether the functioning of flapper valves was speed-sensitive under laboratory conditions. In a residential refrigerator/freezer compressor, different valve motion speeds were observed. Using laser Doppler velocimetry, the velocity of a spot on the flapper close to the port's center was determined. These velocity data were numerically integrated to estimate displacement as a function of crank angle for each speed. There was an attempt to establish a correlation between compressor speed and any activity that might either boost compressor performance or reduce valve life.

For a single working state, Gasche et al.[9] investigated the fluid-structure interaction issue in a model of a reed suction valve with a diameter ratio of 1. The fluid-structure interaction issue was studied by employing a very precise optical sensor to identify the reed's exact position. Orifice inlet values between 20,00 and 12,000 were used to determine the Reynolds number. Even at the required constant mass flow rates, the reed did not reach equilibrium due to hydrodynamic instabilities in the flow. The results showed that the frequency of reed motion was determined by the Reynolds number and dropped dramatically with increasing Reynolds number.

With one-, two- and three-dimensional models, Pereira et al.[10] analyzed the performance of small reciprocating refrigeration compressors. A single-degree-of-freedom model of the valve dynamics was used in each case, with the governing flow equations discretized through a finite volume method. The dynamics of the valve and the flow field as a function of time were solved at the same time. The accuracy of each model was measured against real-world data. The 3D formulation let us model the compressor with its real suction and discharge geometries, and it provided a reference point for testing whether or not simpler, less computationally expensive models can accurately predict the compressor's performance.

Diniz et al.[11] studied the performance of hermetic reciprocating compressors under specific refrigeration settings. The mass flow rate and evaporating and condensing pressures were measured while the compressor was

instrumented with thermocouples in chosen components and pressure transducers to create a pV diagram of the compressor's operation. Despite a general trend toward higher volumetric and thermodynamic efficiencies at lower ambient temperatures, the data demonstrated that the compressor's total efficiency remained almost the same. The acquired pV diagrams showed that when condenser pressure was raised, the influence of pressure waves like overshoot and flutter in the discharge line grew, whereas as evaporation pressure was raised, suction line losses grew.

Using a strain gauge, Nagata et al.[12] monitored the velocity of the suction valve of a hermetic reciprocating compressor for a household refrigerator. Due to the viscosity of the lubrication oil, the motion of the valve at a low rotational speed was highly variable. It was discovered that the movement of the suction valve affects the volumetric efficiency. The number of valve vibrations over the suction port led the volumetric efficiency to fluctuate periodically concerning the compressor's operating speed.

Rigola et al.[13] experimentally investigated the thermal and fluid behaviors of a hermetic reciprocating compressor for household appliances. pV diagram and thermal map of compressor obtained operating with R134a to validate mathematic model of it. Pressures were measured by using three piezoresistive pressure sensors in the suction muffler, compression chamber and discharge plenum while crank angle was measured using a quadrature incremental encoder. Compression, discharge, expansion and suction work process were measured for single compressor speed by changing evaporation temperature. These work processes increased by increasing evaporating temperature and mathematical model developed by them agreed with the experimental results.

Longo and Gasparella[14] experimentally investigated domestic reciprocating compressor operating with R134a to validate their numerical model. One-dimensional model of the reed valves was evolved, and balance equations were applied to conclude the mass, pressure and temperature behavior and the heat and work transfer through the compression process. Suction line thermodynamic losses increased, and total compressor losses were decreased by increasing evaporating temperature.

Posch et al.[6] examined the mechanical and thermodynamic losses of a hermetic reciprocating compressor under ASHRAE operating conditions. The losses of the compressor were represented as entropy production and exergy loss. By reducing the temperature of the valve plate, the cooling capacity and COP of the compressor are raised by 2.63 and 1.57%, respectively. Electrical and gas path losses were the two most prominent losses in a hermetically sealed reciprocating compressor. Higher refrigerant density causes a modest increase in compressor effort, whereas increasing oil viscosity increased mechanical losses by 15.7%. The suction valve had the highest exergy losses of the compressor, whereas the other sections, such as the suction line, the cylinder, the discharge valve and the discharge muffler, had comparable proportions.

Santos et al.[15] examined a linear compressor working without lubricating oil and reported isentropic efficiency for the mechanical and thermodynamic losses. The effects of design parameters such as compressor speed, piston oscillation amplitude, pressure ratio and radial clearance on the volumetric and isentropic efficiencies were investigated, and by varying the radial clearance value from 2.5 to 10 μm, the volumetric efficiency decreased by 2.5% and increased by 4.2%. The parametric analysis revealed that the isentropic efficiency of a compressor was ranked from lowest to highest at the discharge line, suction line and piston cylinder gap, respectively.

Perez-Segarra et al.[16] numerically studied the volumetric and isentropic efficiencies of the hermetic reciprocating compressor. Reducing the compression ratio caused the increasing suction line losses and brought out the increased overshoot in the discharge line of the compressor. Another indication from the study is that increasing the compression ratio up to 10.08 increased the compressor's isentropic efficiency. Moreover, the isentropic efficiency of suction line was higher than the isentropic efficiency of discharge line.

As a result of the literature review above, compressor measurements have been mostly conducted in a laboratory environment with a single-speed compressor. Apart from these ones, measurements of this study were conducted by using a calorimeter test unit in a household appliance producer's research center under ASHRAE (54.4°C/−23.3°C) and additional specific working conditions of (40°C/−25°C), (25°C/−20°C) and (35°C/−15°C) with different operating speeds (1300, 1600, 2100 and 3000 rpm) of a recently developed compressor working with R600a to reflect the realistic situation. Another aspect that makes this study noteworthy is that it focuses on low-speed domestic refrigerant compressors, whereas high-speed industrial compressors tend to dominate the literature. In general, the most important contributions of this investigation are the proposal of measurement for the pV indication diagram and a method for calculating the suction and discharge losses for hermetic reciprocating compressors used in household refrigerators. It is essential for designers to determine the performance losses and evaluate the performance of the compressor in different climatic conditions during research and development duration before the good's serial production. Moreover, the cooling capacity, COP and power consumption metrics should be examined at different operating temperatures since the performance of the compressor will vary depending on the operating condition. Consequently, researchers interested in determining the performance losses of hermetic reciprocating compressors under different operating conditions may find the results of this study useful. Finally, this experimental investigation has been accomplished in cooperation with a leading household producer.

Experimental methodology

Details of investigated compressor

Figure 1 depicts the typical components of a hermetic reciprocating compressor, including the flow regulating

assembly, kit assembly, enclosure, vibration dampening elements and electrical assembly elements. Flow regulation group components include a suction muffler, a cylinder cover, gaskets, a valve plate, suction and discharge valves, a lift limiter and the connections between these pieces of equipment. Grouping components of the kit include the crankshaft, connection rod, piston, body and piston pin. Electrical group components include rotor and stator. While the body fits the majority of the compressor's components, the housing protects and seals all components from the outside environment through the compressor's suction pipe, and the refrigerant at evaporation pressure and superheated vapor temperature enters the compressor.

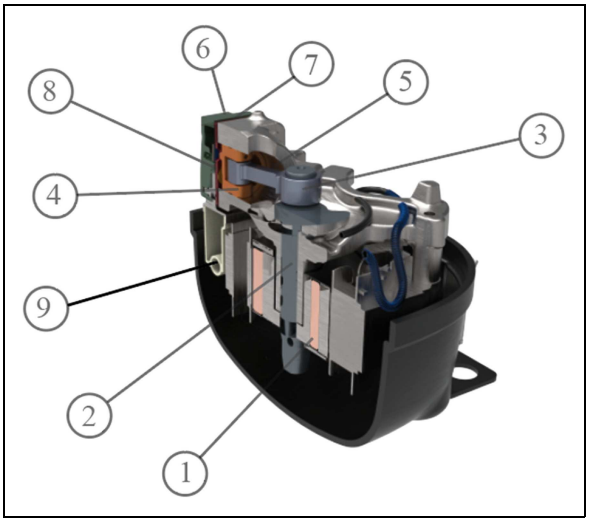


Figure 1. Schematic illustration of the investigated compressor: (1) motor, (2) crankshaft, (3) connecting rod, (4) piton, (5) cylinder, (6) cylinder head, (7) gasket, (8) valve plate and (9) suction muffler.

The refrigerant in the path of the suction muffler's superheated vapor phase collects in the suction port. When the piston goes from the top dead center (TDC) position to the bottom dead center (BDC) position, the cylinder pressure begins to fall. When the gas pressure in the suction manifold is higher than the gas pressure in the cylinder, the suction valve opens. This is known as the suction phase. The movement of the piston from the bottom dead center to the TDC is known as the compression phase. During this stage, the gas pressure in the cylinder is increased by decreasing its volume. When the gas pressure in the cylinder exceeds that of the discharge manifold, the discharge valve opens, and refrigerant gas begins to flow into the discharge manifold. The refrigerant then exits the compressor via the discharge manifold and discharge tube.

Suction and discharge are the two basic thermodynamic losses during this flow in the compressor. Suction line losses are thermodynamically caused by the suction port and suction muffler, while discharge line losses are caused by the discharge port and discharge plenum. To calculate the thermodynamic losses of a compressor, the pV indication diagrams must be obtained. When comparing the ideal indicator diagram to the empirically determined pV indicator diagram, the differences on the high-pressure side represent the discharge line losses, while the differences on the low-pressure side represent the suction line losses.

Experimental setup

Experimentally acquired thermodynamic losses of the hermetic reciprocating compressor were based on Table 1 ASHRAE and household refrigerator operating conditions. In basic calorimeter tests, the COP of a compressor is calculated by measuring the compressor's

Table 1. Experimental test conditions.

Operating condition	Evaporation temperature/ Pressure (°C)/(Bar)	Condensation temperature/Pressure (°C)/(Bar)	Subcool temperature (°C)	Superheat temperature (°C)	Room temperature (°C)	Compressor speed (rpm)
ASHRAE (54.4°C/ −23.3°C)	−23.3/0.624	54.4/7.61	32.2	32.2	32.2	1300
ASHRAE (54.4°C/ −23.3°C)	−23.3/0.624	54.4/7.61	32.2	32.2	32.2	2100
ASHRAE (54.4°C/ −23.3°C)	−23.3/0.624	54.4/7.61	32.2	32.2	32.2	3000
(25°C/−20°C)	−20/0.725	25/3.507	20	20	20	1300
(25°C/−20°C)	−20/0.725	25/3.507	20	20	20	2100
(40°C/−25°C)	−25/0.584	40/5.312	20	25	25	1300
(40°C/−25°C)	−25/0.584	40/5.312	20	25	25	1600
(35°C/−15°C)	−15/0.885	35/4.64	25	25	25	1300
(35°C/−15°C)	−15/0.885	35/4.64	25	25	25	2100
(35°C/−15°C)	−15/0.885	35/4.64	25	25	25	3000

ASHRAE: American Society of Heating, Refrigerating and Air-Conditioning Engineers.

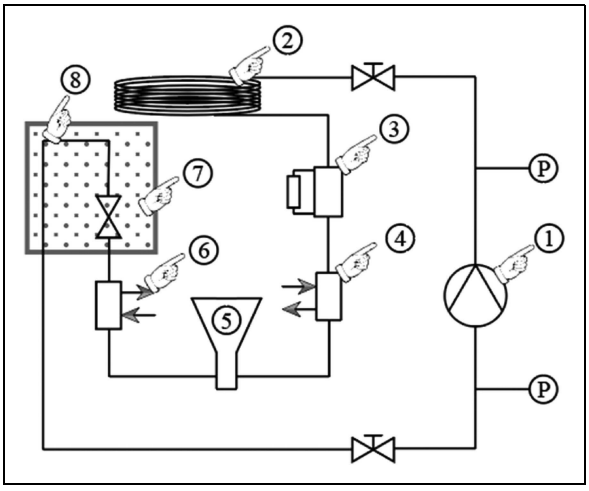


Figure 2. Schematic view of the used calorimeter test unit: (1) compressor, (2) condenser, (3) accumulator, (4) 1st subcool unit, (5) flowmeter, (6) 2nd subcool unit, (7) expansion valve and (8) evaporator.

cooling capacity and power consumption, depending on the operating condition. In calorimetry measurements, it is also possible to monitor the mass flow rate of the refrigerant, the gas temperature at the compressor outlet and the housing surface temperatures.

To evaluate compressors under various operating conditions, calorimeter test rigs are utilized. Figure 2 depicts the cooling system and arrangement of the relevant equipment for the calorimeter test setup utilized in the Arcelik R&D Center Thermodynamic Technologies Laboratory. As shown in the diagram, the test apparatus for the compressor calorimeter was separated into two distinct volumes. In the volume on the right are the compressors to be tested and the equipment used to monitor the suction and output pressures of the compressors. The remaining equipment of the cooling and measurement system is housed in the volume on the left, and both volumes are conditioned to maintain a temperature of room temperature in the interior air. After being compressed in the compressor, the high-pressure, high-temperature refrigerant vapor enters the condenser. For accurate and exact calorimetry measurements, the condensing pressure must be steady. For this reason, a condensed tube heat exchanger with a very high total thermal permeability is utilized as the condenser. The condenser's thermal energy is extracted by pumping cooling water through a temperature-controlled bath.

A proportional–integral–derivative (PID) control device takes the condensation pressure as an input parameter, regulates the electric heater in the bath and maintains the water temperature and, therefore, the condensation temperature at the required value. The liquid refrigerant emerging from the condenser is collected in a container called a battery with a viewing glass. Since the quantity of refrigerant in the other system components will vary depending on the operating conditions, the battery also serves as a refrigerant reservoir. Two subcooling units are present in the calorimeter test configuration.

The first subcooling unit is located right before the mass flowmeter to guarantee that all of the refrigerant entering the flowmeter is in liquid form. The introduction of the refrigerant as a liquid-steam combination into the flowmeter reduces the accuracy of the flowmeter. The objective of the second subcooling unit positioned immediately after the mass flowmeter is to give the subcooling temperature specified by ASHRAE standard[17] with exactitude. Subcooling unit heat exchanger sizing and water conditioning are comparable to the condenser conditioning system. The high-pressure refrigerant is reduced to the desired evaporation pressure by the throttling valve in the pressure vessel in the second chamber of the calorimeter test system after passing through the condenser, the coil, the first subcooling unit, the mass flow meter and the second subcooling unit.

In the evaporator of the aforementioned pressure vessel, the evaporation process takes place. The pressure vessel contains a supplementary heat transfer fluid (R134a), and an electrical heater is positioned slightly below the R134a liquid level. During the functioning of the system, the power supplied to the electric heater is transferred as thermal energy to the secondary fluid, causing some fluid to evaporate. The secondary heat transfer fluid condenses over the evaporator pipes in the top pressure vessel, transferring thermal energy to the real tested fluid and permitting the refrigerant to evaporate. ASHRAE standards stipulate that the superheating degree must reach superheat temperature as a result of evaporation; therefore, the saturation temperature of the secondary fluid is raised to superheat temperature using an electrical heater, and the superheating degree is maintained due to the high heat transfer between the secondary fluid and the tested refrigerant. Since the calorimeter volume in which the pressure vessel is situated is maintained at room temperature, it is believed that there is no heat transfer from the pressure vessel's interior to its outside, and therefore the power supplied by the electric heater is equal to the cooling capacity of the compressor. The ambient temperature of the spaces containing the compressor, the pressure vessel and other components is controlled at room temperature. Cold water supplied by the central cooling unit is cycled through heat exchangers and electrical heaters to accomplish this procedure. The cold water cycling in the heat exchangers is supplied at a constant flow rate, and the PID control circuits, which use the room temperatures as input, regulate the power of the electric heaters to maintain the desired temperature of the two volumes.

The procedures and measurements of the calorimeter test system are controlled and recorded using a personal computer and a data capture system. The thermocouples' analog and digital signals are recorded using a commercial data capture card from National Instruments. A program that manages the whole apparatus is written using LabView® software.

Data reduction

At the beginning of the calorimeter test, the compressor is attached and activated. The compressor is automatically

started until the evaporation and condensation pressures reach the desired value. When all set values determined by the ASHRAE standard become stable for 60 minutes, the arithmetic mean of the values measured over the last 60 minutes is accepted as the calorimeter test result. In the compressor calorimeter test system, the compressor's cooling capacity is determined by two distinct approaches. In the first technique, the mass flow rate determined by the flow meter is multiplied by the enthalpy difference between the evaporator's inlet and outlet:

$$\dot{Q}_e = \dot{m}_r(h_o - h_i) \tag{1}$$

For the calorimeter test to be regarded as genuine, the difference between these two results must be no greater than 2.5%, and the arithmetic mean of the two values for the compressor's cooling capacity is declared. Since the power drawn by the compressor is directly monitored, the following equation is used to compute the cooling efficiency coefficient.

$$\mathrm{COP} = \frac{\dot{Q}_e}{\dot{W}_c} \tag{2}$$

To further clarify the studies conducted in the compressor calorimeter test system, information regarding the stability of the measured quantities throughout the test is offered first. The figures measured during one of the tests conducted under ASHRAE conditions, which correspond to a condensation temperature of 54.4°C and an evaporation temperature of −23.3°C, are displayed graphically. In calorimetry experiments, the stability of the appropriate evaporation and condensation pressures is crucial to the precision of the measurement results.

For this study, the thermodynamic losses of the hermetic reciprocating compressor are separated into suction and discharge lines. Suction line losses are composed of suction muffler and suction port losses, whereas discharge line losses are composed of the discharge port and discharge plenum losses. The losses of the valve plate are expressed as the sum of the suction and discharge line losses. While the loss of the suction muffler is the pressure drop in the muffler, which is one of the suction muffler's design characteristics, the loss of the suction port is the flow losses caused by parameters such as the port diameter, count and coefficient of friction of the suction port. While the definition of discharge port loss is similar to the definition of suction port loss, the discharge plenum loss can be expressed as the loss due to a pressure drop in the discharge plenum of the compressor. In addition to these factors, suction and discharge line losses are also affected by the thickness of the suction and discharge valve leaves, the elasticity modulus, the material and the stiffness value.

By monitoring the instantaneous cylinder volume and pressure, one can derive the pV diagram. To compute compression work, the pV diagram must be integrated and the pV area must be exactly determined. Using the trapezoidal approach, the pV area is calculated. As stated in equation (3), the suction, discharge and cylinder pressures are computed as the average of the 11 cycles' values. Using the cylinder volume and cylinder pressure values, equations (4) and (9) calculate the area of the pV indication diagram. This calculation is utilized to determine the compressor's compression work on the refrigerant. In equations (5) and (10), the area between the measured pV indicator diagram suction line is calcu-lated using the ideal suction pressure curve of the pV indi-cator diagram. This derived field is utilized to calculate the compressor's suction line losses. Using the average suction pressure, average cylinder pressure and cylinder volume, equations (6) and (11) are used to compute the suction port loss of the compressor, and the difference between the suction line and the suction port is calculated as the suction muffler loss. Using the average cylinder pressure, cylinder volume and condensation pressure, equations (7) and (12) are used to compute the area between the ideal condensation pressure and the recorded pV diagram, which is referred to as the discharge line losses. In equations (8) and (13), the average cylinder pressure is utilized to compute discharge port losses using the average discharge pressure and cylinder volume. The discharge plenum loss is the difference between the discharge line losses and the discharge port losses.

$$P = \left(\sum_{i=1}^{11} P\right)_{\mathrm{ave}} \tag{3}$$

$$P_c dV = \left(\frac{P_{c,i} + P_{c,i+1}}{2}\right)(V_i - V_{i+1}) \tag{4}$$

$$(P_c - P_s)dV = \begin{cases} \left(\dfrac{P_{c,i} + P_{c,i+1}}{2}\right)(V_i - V_{i+1}), & P_{c,i+1} < P_s \\ 0, & P_{c,i+1} > P_s \end{cases} \tag{5}$$

$$(P_c - P_d)dV = \begin{cases} \left(\left(\dfrac{P_{c,i} + P_{c,i+1}}{2}\right) - P_d\right)(V_i - V_{i+1}), \\ \qquad P_{c,i+1} > P_d \\ 0, \quad P_{c,i+1} < P_d \end{cases} \tag{6}$$

$$(P_c - P_d)dV = \begin{cases} \left(\left(\dfrac{P_{c,i} + P_{c,i+1}}{2}\right) - P_{e,i+1}\right)(V_i - V_{i+1}), \\ \qquad P_{c,i+1} > P_{e,i+1} \\ 0, \quad P_{c,i+1} < P_{e,i+1} \end{cases} \tag{7}$$

$$(P_c - P_4)dV = \begin{cases} \left(\left(\dfrac{P_{c,i} + P_{c,i+1}}{2}\right) - P_{e,i+1}\right)(V_i - V_{i+1}), \\ \qquad P_{c,i+1} > P_{e,i+1} \\ 0, \quad P_{c,i+1} < P_{e,i+1} \end{cases} \tag{8}$$

$$W_{\mathrm{pV}} = \frac{\int_3^P dV}{\mathrm{rpm}} \tag{9}$$

$$\mathrm{TSL} = \frac{\int (P_3 - P_s) dV}{\mathrm{rpm}} \tag{10}$$

$$\mathrm{TDL} = \frac{\int (P_3 - P_d) dV}{\mathrm{RPM}} \tag{11}$$

$$\mathrm{TSPL} = \frac{\int (P_3 - P_2) dV}{\mathrm{RPM}} \tag{12}$$

$$\mathrm{TEPL} = \frac{\int (P_3 - P_4) dV}{\mathrm{RPM}} \tag{13}$$

Based on the angular position of the crankshaft, the location of the piston and the instantaneous compression volume are calculated using equation (14) during pV experiments. To calculate these data correctly, the position of the piston at the TDC and the angle of the crankshaft must be measured experimentally. Using the compressor design parameters shown in Table 2, the first stage of pV measurement is performed, and the piston position is determined by the various crank angles. Figure 3 depicts the design parameters required to compute piston position relative to different crank angles.[18]

$$z = z_0 + (r + l)\cos\theta_{\mathrm{TDC}} - \left(r\cos\theta + \sqrt{1 - \left(\frac{r}{l}\sin\theta - \frac{e}{l}\right)^2} \right) \tag{14}$$

After calibrating the magnetic encoder and pressure sensors, the measurement setup was prepared in a hermetic reciprocating compressor, and once the system reached the regime in the calorimeter measurement setup, indicator diagram measurements were performed in operating conditions, with data recorded at each crank angle for various operating cycles.

Preparation of the compressor for the experiments

Before starting the pV experiments on the compressor, it is required to make certain preparations. These preparations include putting the pressure sensors in the appropriate locations, mounting the compressor's equipment to the flanged housing, conducting internal and external leakage tests and mounting the encoder. Figure 4 depicts the installation of compressor equipment in a flanged housing. In flanged housing, a bolt-and-nut connection replaces the original housing's method of attachment. Rubber gaskets are utilized to fit the original upper and lower casing surfaces of the compressor. When selecting gaskets, compressive strength is taken into account. Utilizing the gasket channel and rubber gasket on the flange provides a seal. To ensure the integrity of the protractor (encoder) of the crankshaft with the compressor, the upper casing is cut to allow the encoder to pass. To protect the crankshaft protractor, an extra rectangular prism-shaped housing is welded to the upper flanged housing (with the encoder's cut area measurements). The upper casing is welded to flange-cutting plates. The pool immersion method is used to prevent leaks from

Table 2. Investigated compressor's design parameters.

Design parameter	Value
Cylinder bore	24.28 mm
Crankshaft diameter	10.64 mm
Eccentricity	2.25 mm
Connection rod length	38.7 mm
Oil viscosity	10 cSt
Reed valve thickness	0.2 mm

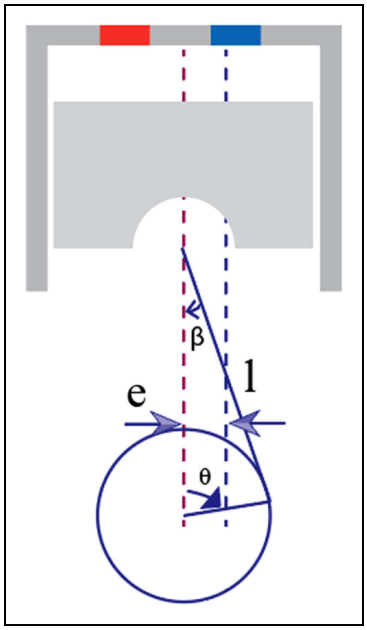


Figure 3. Mechanism motion diagram of a hermetic reciprocating compressor.

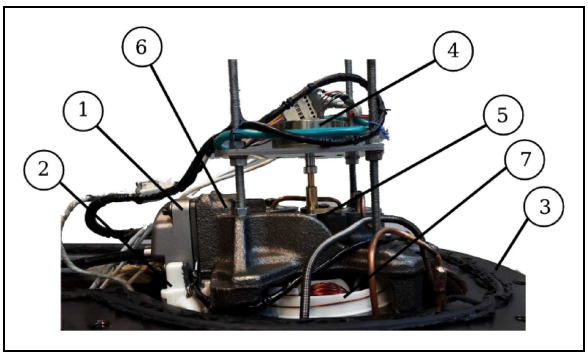


Figure 4. Encoder mounted on the used crankshaft to measure cylinder pressure and volume, synchronously for pV diagram: (1) cylinder cover, (2) suction muffler, (3) housing with flanges, (4) magnetic encoder, (5) crankshaft, (6) body and (7) motor.

the welding penetration areas of the compressor housing, which is linked by welding.

As shown in Figure 4, a magnetic encoder is installed on the crankshaft axis to determine the crankshaft's angle throughout the cycle. The magnetic portion of the non-contact magnetic encoder is bonded to the adhesive spacer. It is mounted on a plate that is secured at three points, preventing the magnetic encoder from being impacted by the rotation of the crank. Two of the three spots where the plate is fixed are often body holes or holes that can be bored in the right position, while the third point is the bolt hole in the discharge muffler volumes. The plate containing the magnetic encoder is attached to the body using studs of adequate length and diameter. The pool immersion method is used to prevent leaks from the welding penetration areas of the compressor housing, which is linked by welding. After the compressor has passed the internal leakage, exterior leakage and impact tests, the lower and upper flanged casing bolts are fastened and closed. The pressure sensors are connected to the data acquisition system using an Ethernet cable with the Category 6 cable (CAT6) standard. The cable connection of the pressure sensors is performed by the relevant sensor's user handbook. The Ethernet cable is connected to the pressure sensors on the compressor using fit true, as shown in Figure 5.

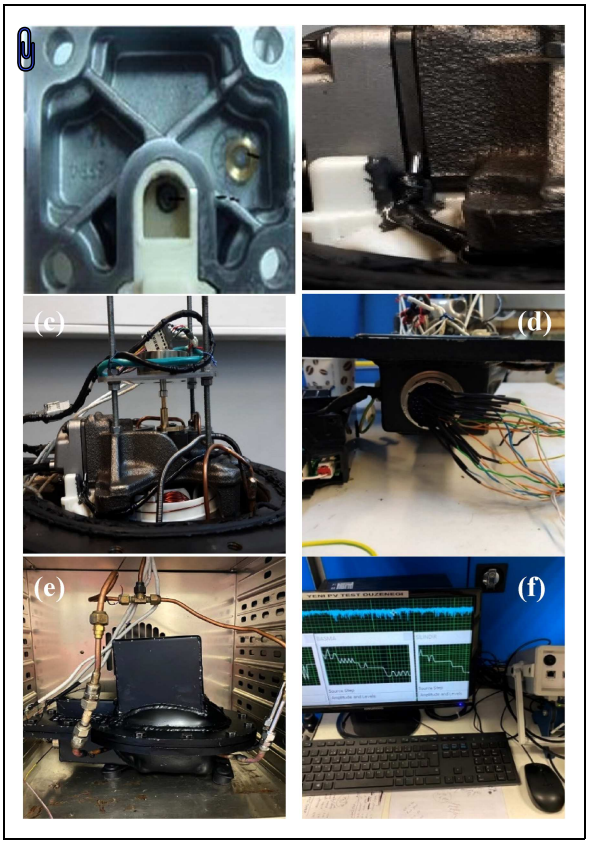


Figure 5. Experimental preparation of stages (a) installation of cylinder and discharge pressure sensor, (b) installation of cylinder pressure sensor, (c) installation of magnetic encoder, (d) connection of sensors on fit true to power supply, (e) hot calibration in ETUV oven and (f) cold calibration in laboratory environment. ETUV: drying oven.

During the compressor's pV measurements, the suction, discharge and cylinder pressure data are measured at various crank angles. As illustrated in Figure 5, the suction, discharge and cylinder pressure sensors are mounted, respectively, in the suction plenum, the cylinder head and where the valve plate opens into the cylinder. Suction, discharge and cylinder pressure sensors are calibrated at elevated and subzero pressure. Cold calibration is performed at ambient temperature, whereas hot calibration is carried out in an drying oven (ETUV) oven set to 80°C. In hot calibration, the ambient and storage temperatures must approach 80°C. The temperature of the enclosure should be measured using a thermal twin. For hot and cold calibration, a three-way manifold manometer, a data collecting device, a process calibration device, a vacuum pump, LabView software and a computer are utilized. When measuring pressure at gauge pressures below atmospheric pressure, a vacuum pump is utilized. A process calibration device and a three-way manifold manometer are utilized for pressures over atmospheric pressure. The voltage on the pressure sensor is read in terms of the pressure provided to the compressor by a three-way manifold manometer utilizing LabView software. Pressure and volume data are measured in volts for the suction, discharge and cylinder pressure sensors by increasing 0.5 Bar between calibration measurements of 0.3–10 Bar. For calibration measurements, the pressure and volume readings are read in volts for the suction, discharge and cylinder pressure sensors by lowering 0.5 Bar between 10 and 0.3 Bar.

One of the interesting aspects of this work is that, unlike earlier systems, magnetic encoders were utilized in this investigation. Oil is transported to the internal structure of the encoder during use, especially depending on the usage time. This corrupts the measurements, makes it impossible to conduct long-term measurements with a single encoder and wastes work and time. Furthermore, when using an optical encoder, the encoder shaft and the component on the crank eccentric journal must be coupled. If this connection is not made carefully, it adds extra strain to the crank and has the potential to destroy the coupling over time. In the active magnetic encoder, non-contact measurement is accomplished. In this regard, there is no shaft bearing area through which oil can pass, therefore couplings are not required. A 1 mm gap is left between the crank eccentric component and the magnetic encoder body for the measurement.

Assuming that the experiment was properly set up and calibrated to avoid any fixed mistakes, there would have been random errors connected with the experimental results. To quantify random mistakes in the data, a non-certainty analysis was performed. Table 3 provides a summary of the uncertainties for each instrument as well as the uncertainty range for the global cooling capacity and COP obtained from observations and error propagation.

Results and discussion

To examine the suction and discharge line loss characteristics of the compressor under different operating conditions,

Table 3. Summary of the measurement and calculation uncertainties.

Parameter	Sensor	Accuracy	Uncertainty
Temperature	Thermocouple	±0.3 K	±0.3 K
Suction pressure	Pressure transducer	±0.1%	0.2–0.4 kPa
Discharge pressure	Pressure transducer	±0.1%	1–2 kPa
Cylinder pressure	Pressure transducer	±0.1%	1–2 kPa
Mass flow rate	Coriolis-effect flow meter	±0.5%	0.5–1.5 mg s^{-1}
Power consumption	Power transducer	±0.1%	0.04–0.06 W
Cooling capacity	–	–	±0.8%
COP	–	–	±0.85%

pV experiments were conducted under four different temperature and pressure conditions, one of which was ASHRAE and three of which were refrigerator operating conditions, and at various compressor speeds. Contrary to research in the literature, it is required to evaluate a refrigerator compressor in various situations, since it operates in varying climatic conditions or seasons. Consequently, it is vital to evaluate the compressor's performance while taking all working conditions into consideration. The thermodynamic losses of the hermetic reciprocating compressor were determined in this work by experimentally measuring the pV indication diagram under the operating parameters shown in Table 1 as well as temperature and pressure readings at the prescribed points.

Figure 6 depicts the change in cylinder capacity as a result of varying stroke volume. Observations indicate that the thermodynamic losses of the compressor grow

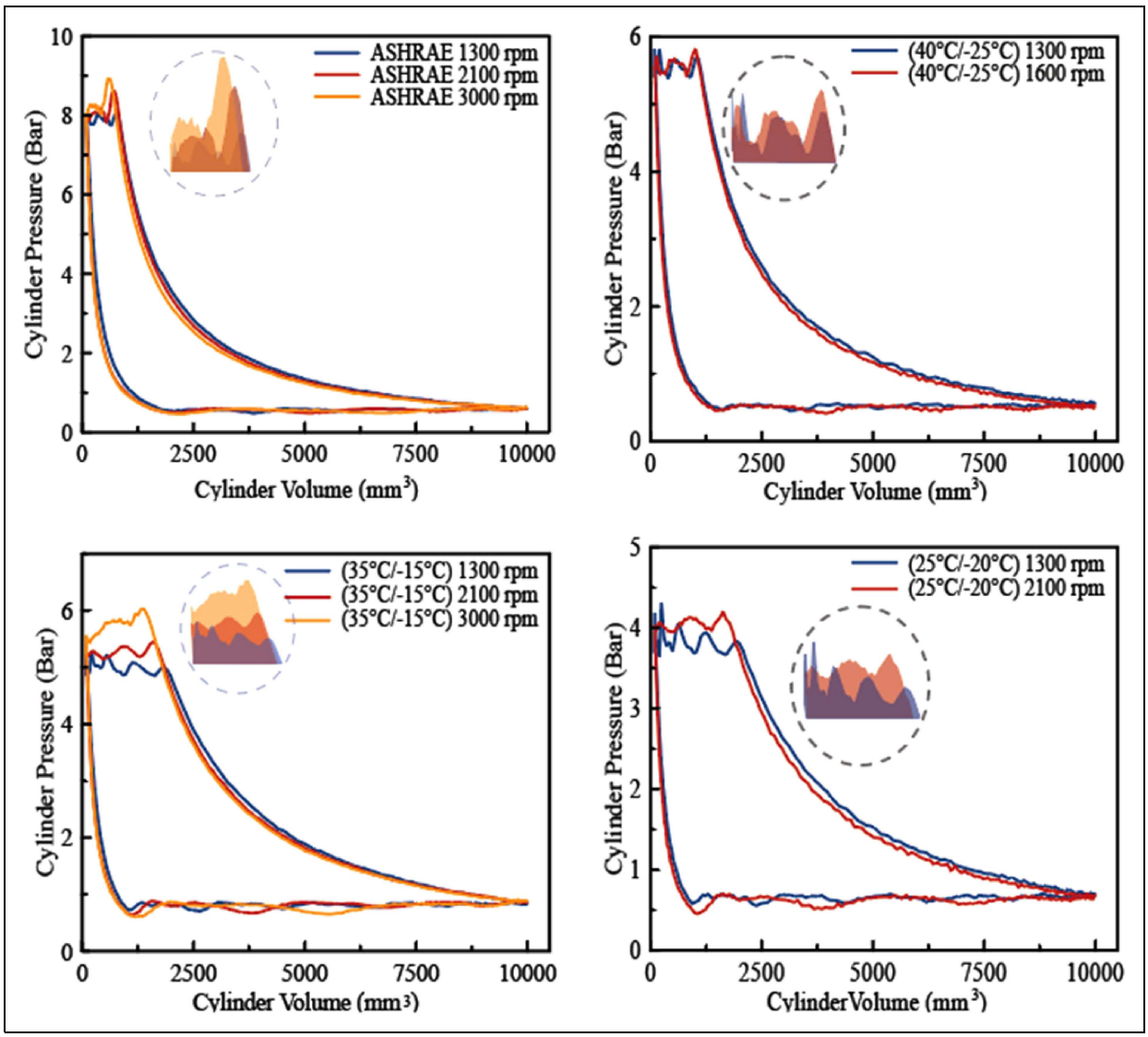


Figure 6. Investigated compressor's obtained pV indication diagrams (a) ASHRAE (54.4°C/−23.3°C), (b) (40°C/−25°C), (c) (35°C/−15°C) and (d) (25°C/−20°C). pV: pressure-volume; ASHRAE: American Society of Heating, Refrigerating and Air-Conditioning Engineers.

with increasing compressor speed, with discharge pressure loss dominating under all working conditions. As shown in Figure 6, compressor thermodynamic losses are proportional to compressor speed, as they are proportional to an increase in compressor speed and, thus, mass flow rate. Due to the increasing mass flow rate with increasing compressor speed, the pressure loss that happens in the compressor based on the design specifications increases the compressor's thermodynamic losses, since the compressor speed is indirectly related to losses. With the opening of the valve leaf, the refrigerant compressed to a high pressure in the cylinder causes pressure fluctuations and turbulent flow in the discharge manifold, which contributes to the increased discharge losses of the compressor. In accordance with the obtained results of the current study, Mohammadi-Amin et al.[18] indicated that raising compressor speed increases compression work and thermodynamic losses.

The region beneath the pV indication curve of the compressor indicates the compression work performed by the compressor. It has been determined that the compression work performed by the compressor increases naturally with increasing compressor speed as shown in Figure 6. Examining the suction and discharge line losses reveals that the suction and discharge losses rise as compressor speed increases. Suction line losses are the total of the suction muffler and suction port losses and appear to be directly connected to evaporation pressure. Suction losses also depend on the design of the suction muffler, the characteristics of the suction port and the material and mechanical qualities of the suction valve. Discharge line losses consist of the discharge port and discharge plenum losses. These losses are attributable to features including pressure oscillations in the discharge line, the characteristics of the discharge port and the mechanical qualities of the discharge valve leaf. Rigola et al.[13] have investigated the reciprocating compressor at a single speed by changing the evaporating temperature using R134a and they demonstrated increasing suction line losses when increased evaporation temperature. Longo

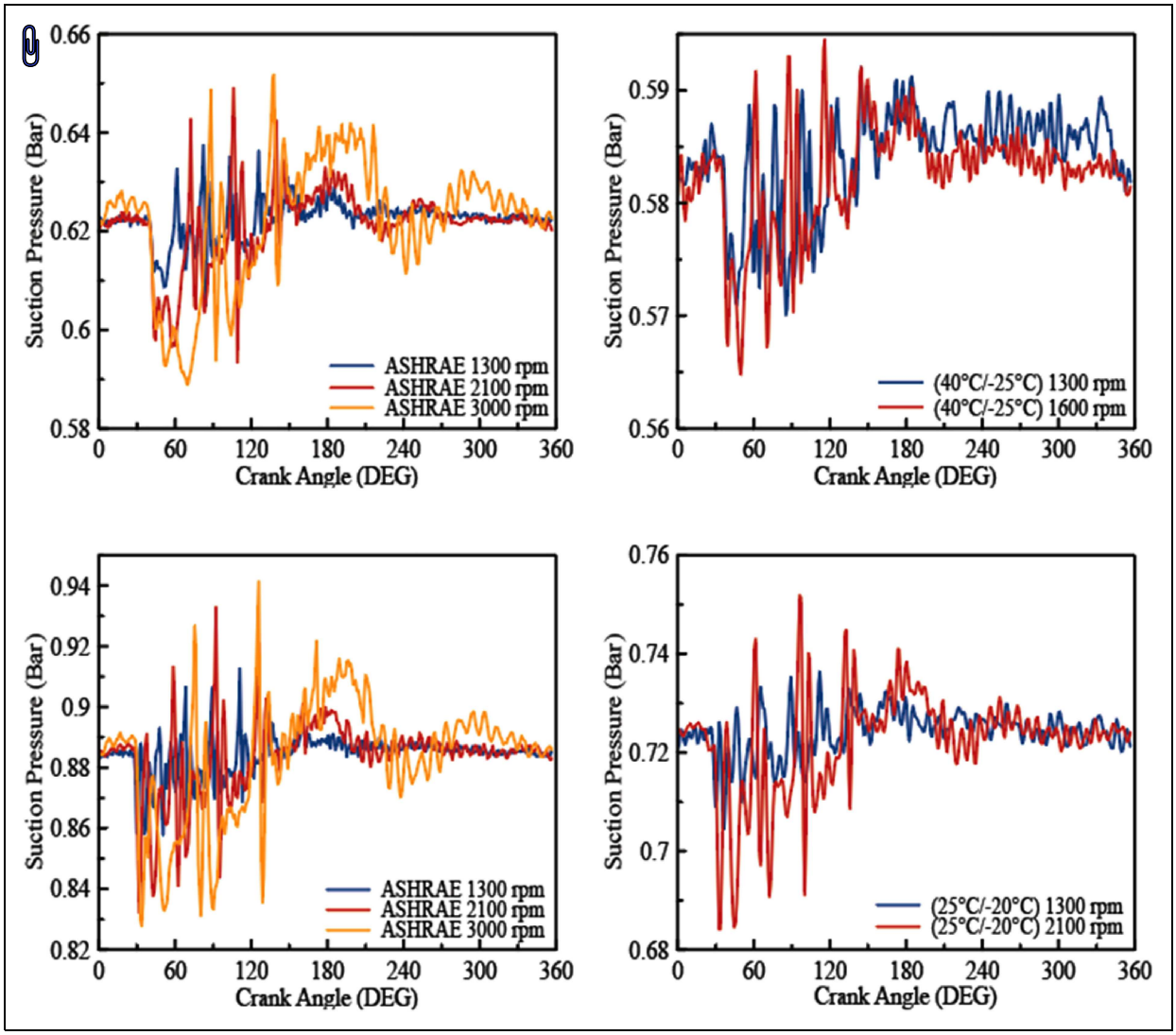


Figure 7. Investigated compressor's obtained suction pressure diagrams (a) ASHRAE (54.4°C/−23.3°C), (b) (40°C/−25°C), (c) (35°C/−15°C) and (d) (25°C/−20°C). ASHRAE: American Society of Heating, Refrigerating and Air-Conditioning Engineers.

Table 4. Suction and discharge stages.

Operating condition	Compressor speed (rpm)	Open/Close time of suction valve (°)	Average pressure amplitude variation (%)	Duration of suction valve leaf opening (ms)	Duration of the suction stage (ms)	Duration of discharge stage (ms)
ASHRAE (54.4°C/−23.3°C)	1300	52/127	3.11	5.00	16.41	3.72
ASHRAE (54.4°C/−23.3°C)	2100	58/141	4.58	3.57	10.16	2.22
ASHRAE (54.4°C/−23.3°C)	3000	70/147	6.44	2.78	7.00	1.61
(25°C/−20°C)	1300	30/137	2.23	4.87	18.21	6.15
(25°C/−20°C)	2100	33/141	5.14	3.57	17.82	4.05
(40°C/−25°C)	1300	47/146	2.43	4.62	17.31	3.59
(40°C/−25°C)	1600	50/150	3.02	4.79	14.69	3.02
(35°C/−15°C)	1300	30/134	2.66	6.54	18.46	6.15
(35°C/−15°C)	2100	32/133	5.93	5.71	11.59	3.89
(35°C/−15°C)	3000	34/135	8.31	2.94	7.83	2.72

ASHRAE: American Society of Heating, Refrigerating and Air-Conditioning Engineers.

and Gasparella[14] have studied the reciprocating compressor operating at different evaporating temperature using R134a and they illustrated total compressor losses decreases when evaporating temperature increases. Diniz et al.[11] found that increasing condensing and evaporating pressure increases thermodynamic losses, which is in agreement with the findings of the present investigation. As a result, it can be clearly seen that these investigations' outputs support those in the current study.

Figure 7 depicts the suction pressure diagrams of the compressor under various operating conditions based on the crankshaft angle. Table 4 displays the opening and shutting periods of the suction and discharge valve leaves, as well as the suction and discharge process times and the suction valve's pressure amplitude. It was determined that when the compressor speed increased, the pressure amplitude of the suction plenum increased and the duration of suction and discharge stages decreased. With increased compressor speed, a delay in the first opening time of the suction valve leaf is seen. The pressure amplitude of the initial flutter movement is substantially greater than that of the subsequent flutter movement, which can be interpreted as the influence of the pulsatile flow being observed in the first flutter movement. After the final fluttering motion of the suction valve leaf, the pressure change in the compressor occurs often and with a small amplitude. This is likely due to oscillations in the flow after the suction valve leaf has been entirely closed.

Figure 8 depicts the discharge pressure diagrams of the compressor under various operating conditions based on the crankshaft angle. Under all conditions of operation, the discharge pressure peaks at a specific pressure value and then declines and equalizes with the discharge pressure. It is observed that the degree of this peak point, known as overshoot, increases as the compressor's speed increases. As depicted in Figure 8, pressure oscillations in the discharge valve leaf persist throughout the whole discharge process due to pulsatile flow in the compressor, regardless of the operating condition and compressor speed. Table 4 demonstrates that the suction and discharge process times decrease as compressor speed increases. According to the findings of the present investigation, Rigola et al.[13] illustrated the pV indicator diagrams by changing evaporating temperature. These overshoot and flutter effects are more apparent when the evaporating temperature decreases. The overshoot effect was observed to grow with condensing by Diniz et al.[11] which is consistent with the results of the current study.

Calculating the suction and discharge losses of the hermetic reciprocating compressor requires using equations (4)–(14). Figure 9 depicts the suction port, suction muffler, discharge port and discharge plenum losses under various operating conditions for the investigated compressor. This loss analysis, which is one of the research that takes this study to the forefront, identifies the compressor efficiency-reducing characteristics. The compressor's thermodynamic losses are divided into suction and discharge losses. The suction losses consist of the suction port and suction muffler, whereas the discharge losses consist of the discharge port and discharge plenum losses. By stressing these losses, a contribution to the literature has been made. As seen in Figure 9, these stipulated suction and discharge losses rise as compressor speed increases. The suction port has the highest rate of these losses, whereas the suction muffler has the lowest. The low thermodynamic losses in the suction muffler are attributable to the suction muffler's design and have the low values expected for a well-designed muffler. The largest proportion of discharge line losses is caused by the discharge port, and these losses are dependent on the discharge port's design characteristics, valve leaf movements,

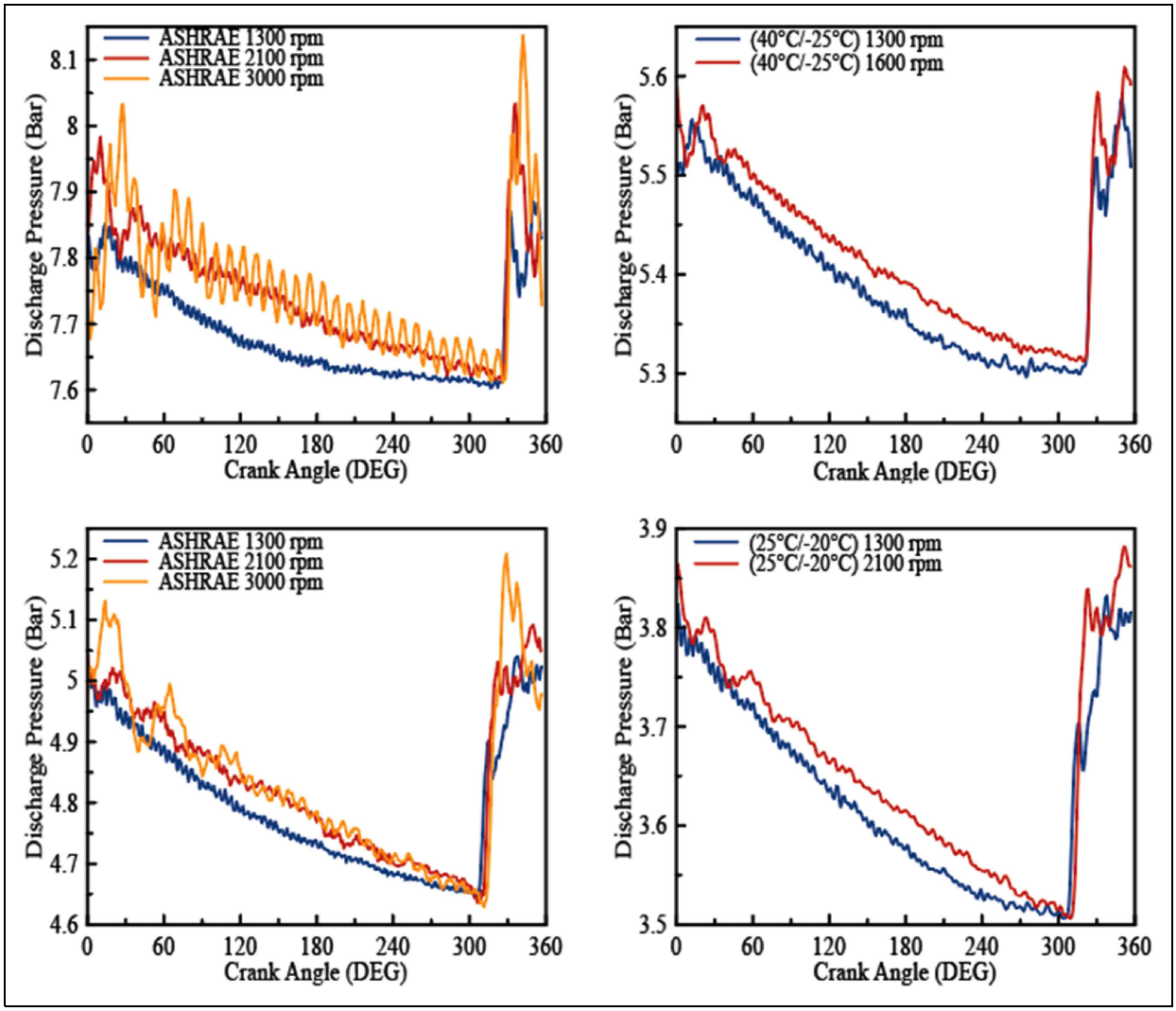


Figure 8. Investigated compressor's obtained discharge pressure diagrams (a) ASHRAE (54.4°C/−23.3°C), (b) (40°C/−25°C), (c) (35°C/−15°C) and (d) (25°C/−20°C). ASHRAE: American Society of Heating, Refrigerating and Air-Conditioning Engineers.

compressor speed and operating pressure. As anticipated, the discharge port losses grow as the compressor's speed and, consequently, mass flow rate increase. While discharge port losses increase proportionally as condensation pressure rises, suction port losses increase proportionally as evaporation pressure rises. It has been discovered that as evaporation and condensation pressures increase, the gas forces and port losses increase due to the effects of pulsatile flow. Engel and Deschamps[19] have examined thermodynamic losses of the reciprocating compressor using different fluids, showed similar trends and obtained comparable results with those in the current study.

Conclusion

Determination of the performance losses and evolution the performance of the compressor is ought to be performed for different climatic conditions. In this study, thermodynamic losses of a newly designed hermetic reciprocating compressor operating with R600a under various conditions of operation are determined by using a calorimetric test unit differently from the others in the literature. In general, the most important contributions of this article are the proposal of measurement for the pV indication diagram and a method for calculating the suction and discharge losses for hermetic reciprocating compressors used in household refrigerators operating with R600a. Researchers interested in determining the performance losses of hermetic reciprocating compressors are supposed to benefit from the outcomes of this study. The current experimental investigation is a result of university and industry collaboration; therefore, it should be considered as one of the successful samples. The following listed items are the most important findings from the research conducted.

1. Pulsatile flow is the dominant irreversibility that affects compressor performance. Examination of both the suction pressure curves and the discharge phase of the indicator diagram revealed which pressure wave was an overshoot and which was a flutter in the suction and discharge lines. These obtained flow

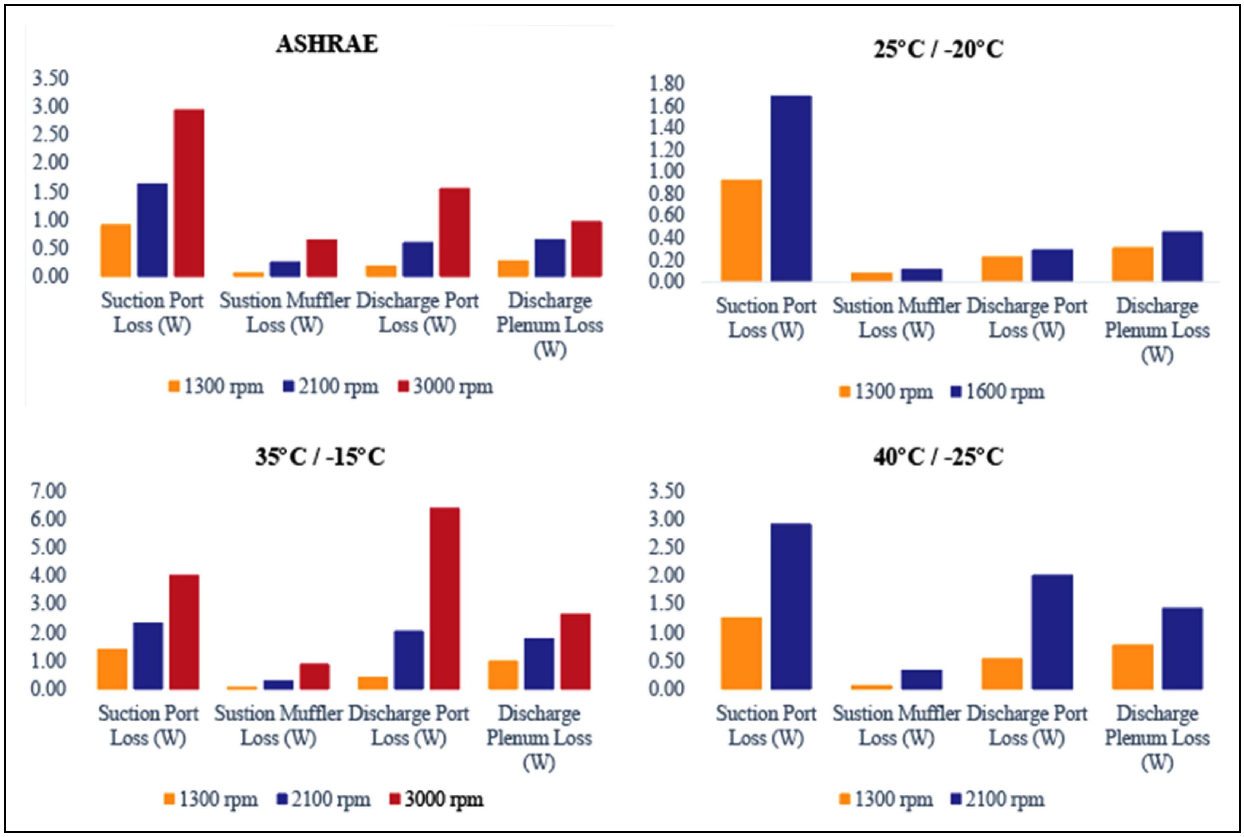


Figure 9. Investigated compressor's obtained thermodynamic losses (a) ASHRAE (54.4°C/−23.3°C), (b) (40°C/−25°C), (c) (35°C/−15°C), (d) (25°C/−20°C). ASHRAE: American Society of Heating, Refrigerating and Air-Conditioning Engineers.

characteristics were a proof of pulsatile flow in the compressor.

2. Magnetic measurement of crank angle for hermetic reciprocating compressors was presented. Suction, discharge and cylinder pressures were measured concurrently using the data from a magnetic encoder. The obtained results helped the calculation of compressor compression work, suction and discharge line losses.
3. The variation of empirically determined suction and discharge pressures concerning ASHRAE (54.4°C/−23.3°C) and additional specific working conditions of (40°C/−25°C), (25°C/−20°C) and (35°C/−15°C) were calculated to examine the effect of operating conditions on pressure fluctuations and reflect the realistic situation. Although the pressure fluctuations were significantly low in the ASHRAE working condition assumed as the regulatory acceptance standard, an increase in pressure fluctuations was noticed in the additional refrigerator operating conditions, which has a negative impact on the operation of the compressor. The obtained result indicated that compressor performance tests should be performed considering additional refrigerator operating conditions.
4. A significant portion of the losses, occurred in the suction and discharge lines, was caused by the parameter of port losses. This is due to the fact that they will be decreased with increasing the number of ports as well as the characteristics of the suction and discharge valves. Therefore, these issues need to be taken into consideration to reduce the compressor's thermodynamic losses. The suction line losses having the largest losses in the compressor were calculated as 50.1%, 50.9%, 64.9% and 67.9% of the total compressor losses, and it has been determined that they increased with increasing the condensation pressure.
5. It was obtained that the condensation pressure has an inverse characteristic with the suction and discharge line losses. For this reason, it is essential to design and assess the compressor according to low condensation pressure. Total compressor losses increased with decreasing the condensation pressure. These losses were 10%, 8.7%, 5.7% and 4.6% of the total work and they were observed at the same speed of 1300 rpm as the lowest one under all operating conditions.
6. The fundamental performance characteristics of the compressor were determined experimentally, and the factors that influenced these parameters were clarified.

Acknowledgements

The authors would like to thank Arcelik A.Ş. for their support during the experimental research. This study is based on the PhD dissertation completed at Yıldız Technical University.

Declaration of conflicting interests

The author(s) declared no potential conflicts of interest with respect to the research, authorship and/or publication of this article.

Funding

The author(s) received no financial support for the research, authorship and/or publication of this article.

ORCID iD

Aykut Bacak https://orcid.org/0000-0003-3157-1992

References

1. Wu W, Jian Z, Song M, et al. Study of valve motion in reciprocating refrigerator compressors based on the 3-d fluid structure interaction model. In: Proceedings of international compressor engineering conference, Purdue, West Lafayette, USA, 2016, paper no. 1523.
2. Real MA and Pereira EAG. Using pV diagram synchronized with the valve functioning to increase the efficiency on the reciprocating hermetic compressors. In: Proceedings of international compressor engineering conference, Purdue, West Lafayette, USA, 2010, paper no. 1225.
3. Jin H, Sun Z, Gu J, et al. A detrending-extracting-zooming-based speed measurement method for hermetic reciprocating compressor. *Measurement* 2020; 157: 107654.
4. Egger A, Almbauer R, Dür L, et al. Multi-Response optimization applied to a mechanically assisted reed valve of a hermetic reciprocating compressor. *Int J Refrig* 2020; 119: 119–130.
5. Silva E and Dutra T. Piston trajectory optimization of a reciprocating compressor. *Int J Refrig* 2021; 121: 159–167.
6. Posch S, Hopfgartner J, Dür L, et al. Thermal loss analysis of hermetic compressors using numerical simulation. *Appl Therm Eng* 2018; 130: 1580–1589.
7. Zhao B, Jia X, Sun S, et al. FSI Model of valve motion and pressure pulsation for investigating thermodynamic process and internal flow inside a reciprocating compressor. *Appl Therm Eng* 2018; 131: 998–1007.
8. Lenz JR and Collings DPE. A study of flapper valve motion in a variable speed compressor. In: Proceedings of international compressor engineering conference, Purdue, West Lafayette, USA, 2010, paper no. 1343.
9. Gasche JL, Arantes DM and Andreotti T. Experimental analysis of the fluid structure interaction in a suction valve model. In: Proceedings of international compressor engineering conference, Purdue, West Lafayette, USA, 2014, paper no. 1217.
10. Pereira ELL, Deschamps CD and Ribas FA. A comparative analysis of numerical simulation approaches for reciprocating compressors. In: Proceedings of international compressor engineering conference, Purdue, West Lafayette, USA, 2008, paper no. 1303.
11. Diniz MC, Melo C and Deschamps CJ. Experimental performance assessment of a hermetic reciprocating compressor operating in a household refrigerator under on–off cycling conditions. *Int J Refrig* 2018; 88: 587–598.
12. Nagata S, Nozaki T and Akizawa T. Analysis of dynamic behavior of suction valve using strain gauge in reciprocating compressor. In: Proceedings of international compressor engineering conference, Purdue, West Lafayette, USA, 2010, paper no. 1273.
13. Rigola J, Raush G, Perez-Segarra CD, et al. Detailed experimental validation of the thermal and fluid dynamic behavior of hermetic reciprocating compressors. *HVAC and R Res* 2004; 10: 291–306.
14. Longo GA and Gaparella A. Unsteady state analysis of the compression cycle of a hermetic reciprocating compressor. *Int J Refrig* 2003; 26: 681–689.
15. Santos CJ, Dutra T and Deschamps CJ. Scrutinizing the sources of inefficiencies in the piston-cylinder clearance of an oil-free linear compressor. *Int J Refrig* 2019; 104: 513–520.
16. Perez-Segarra CD, Rigola J, Soria M, et al. Detailed thermodynamic characterization of hermetic reciprocating compressors. *Int J Refrig* 2005; 28: 579–593.
17. American Society of Heating, Refrigerating and Air-Conditioning Engineers. Methods of testing for rating positive displacement refrigerant compressors and condensing units. 1993.
18. Mohammadi-Amin M, Jahangiri AR and Bustanchy M. Thermodynamic modeling, CFD analysis and parametric study of a near-isothermal reciprocating compressor. *Therm Sci Eng Prog* 2020; 19: 100624.
19. Engel RC and Deschamps CJ. Comparative analysis between the performances of reciprocating and rolling piston compressors applied to a domestic heat pump water heater. *Int J Refrig* 2019; 102: 130–141.

Nomenclature

e	Eccentricity (m)
f	Compressor operating frequency (Hz)
h_i	Inlet enthalpy (J/kg)
h_o	Outlet enthalpy (J/kg)
l	Connecting rod length (m)
m_{ideal}	Ideal mass flow rate (kg/s)
m_r	Refrigerant mass flow rate (kg/s)
r	Crankshaft radius (m)
z	Location (m)
z_0	Top dead center location (m)
Q_e	Evaporation capacity (W)
P	Pressure (Bar)
P_c	Cylinder pressure (Bar)
P_s	Suction pressure (Bar)
P_d	Discharge pressure (Bar)
$P_{c,I}$	Pressure at the first crank angle (Bar)
V_c	Compressor volume (m^3)
V_i	Volume at the first crank angle (m^3)
W_c	Power consumption (W)
η_v	Volumetric efficiency (%)
θ_{TDC}	Angle of the crankshaft (°)
$\rho_{c,i}$	Refrigerant density at the compressor inlet (kg/m^3)

Abbreviations

ASHRAE	American Society of Heating, Refrigerating and Air-Conditioning Engineers
BDC	Bottom dead center
CAT6	Category 6 cable
CFD	Computational fluid dynamics
COP	Coefficient of performance
DES	Detached eddy simulation
DEZ	Detrending extracting zooming
ETUV	Drying oven
FSI	Fluid-structure interaction
OPT	Optimal piston trajectory
PID	Proportional integral derivative

pV	Pressure-volume
RNG	Re-normalization group
rpm	Rotation per minute
TDC	Top dead center
TDL	Total discharge loss
TEPL	Total discharge plenum loss
TSL	Total suction loss
TSPL	Total suction port loss